Research Article | Vol. 7, No. 11 | 1 Nov 2016 | BIOMEDICAL OPTICS EXPRESS 4581

Biomedical Optics EXPRESS

Thermal therapy with magnetic nanoparticles for cell destruction

ADI VEGERHOF,[1] MENACHEM MOTEI,[1] ARKADY RUDINZKY,[1] DROR MALKA,[2] RACHELA POPOVTZER,[1] AND ZEEV ZALEVSKY[1,*]

[1]*Faculty of Engineering & the Institute of Nanotechnology and Advanced Materials, Bar-Ilan University, Ramat-Gan, Israel*
[2]*Faculty of Engineering Holon Institute of Technology, Holon, Israel*
[*]*zalevsz@biu.ac.il*

Abstract: In this article we suggest a new concept for cell destruction based upon manipulating magnetic nanoparticles (MNPs) by applying external, low frequency alternating magnetic field (AMF) that oscillates the particles, together with focused laser illumination. Assessment of temperature profiles in a head and neck squamous cell carcinoma sample showed that cells with MNPs, treated with AMF (3 Hz, 300 mW) and laser irradiation (30 mW), reached 42°C after 4.5 min, as opposed to cells treated with laser but without AMF. Moreover, a theoretical model was developed to assess the overall theoretical temperature rise, which was shown to be 50% lower than the experimental temperature. Furthermore, we found that the combination of laser irradiation and AMF decreased the number of live cells by ~50%. Thus, the concentrated assembly of laser heating with AMF-induced MNP oscillations leads to more rapid and efficient cell death. These results suggest that the manipulated MNP technique can serve as a superior agent for PTT, with improved cell death capabilities.

OCIS codes: (140.3538) Lasers, pulsed; (140.7300) Visible lasers; (170.1420) Biology; (170.1470) Blood or tissue constituent monitoring; (170.1530) Cell analysis.

References and links

1. X.-L. Yue, F. Ma, and Z.-F. Dai, "Multifunctional magnetic nanoparticles for magnetic resonance image-guided photothermal therapy for cancer," Chin. Phys. B **23**(4), 044301 (2014).
2. X. Huang, I. H. El-Sayed, W. Qian, and M. A. El-Sayed, "Cancer cells assemble and align gold nanorods conjugated to antibodies to produce highly enhanced, sharp, and polarized surface Raman spectra: a potential cancer diagnostic marker," Nano Lett. **7**(6), 1591–1597 (2007).
3. L. Soustelle, B. Aigouy, M.-L. Asensio, and A. Giangrande, "UV laser mediated cell selective destruction by confocal microscopy," Neural Dev. **3**(1), 11 (2008).
4. I. Marcos-Campos, L. Asín, T. E. Torres, C. Marquina, A. Tres, M. R. Ibarra, and G. F. Goya, "Cell death induced by the application of alternating magnetic fields to nanoparticle-loaded dendritic cells," Nanotechnology **22**(20), 205101 (2011).
5. A. Ito and T. Kobayashi, "Intracellular Hyperthermia Using Magnetic Nanoparticles : A Novel Method for Hyperthermia Clinical Applications," Therm. Med. **24**(4), 113–129 (2008).
6. A. Ito, M. Shinkai, H. Honda, and T. Kobayashi, "Medical application of functionalized magnetic nanoparticles," J. Biosci. Bioeng. **100**(1), 1–11 (2005).
7. V. S. Kalambur, B. Han, B. E. Hammer, T. W. Shield, and J. C. Bischof, "In vitro Characterization of Movement, Heating and Visualization of Magnetic Nanoparticles for Biomedical Applications," Nanotechnology **16**(8), 1221–1233 (2005).
8. M. Kawashita, S. Domi, Y. Saito, M. Aoki, Y. Ebisawa, T. Kokubo, T. Saito, M. Takano, N. Araki, and M. Hiraoka, "In vitro heat generation by ferrimagnetic maghemite microspheres for hyperthermic treatment of cancer under an alternating magnetic field," J. Mater. Sci. Mater. Med. **19**(5), 1897–1903 (2008).
9. X. Huang, I. H. El-Sayed, W. Qian, and M. A. El-Sayed, "Cancer cell imaging and photothermal therapy in the near-infrared region by using gold nanorods," J. Am. Chem. Soc. **128**(6), 2115–2120 (2006).
10. A. W. Sainter, T. A. King, and M. R. Dickinson, "Effect of target biological tissue and choice of light source on penetration depth and resolution in optical coherence tomography," J. Biomed. Opt. **9**(1), 193–199 (2004).
11. M. Johannsen, U. Gneveckow, B. Thiesen, K. Taymoorian, C. H. Cho, N. Waldöfner, R. Scholz, A. Jordan, S. A. Loening, and P. Wust, "Thermotherapy of Prostate Cancer Using Magnetic Nanoparticles: Feasibility, Imaging, and Three-Dimensional Temperature Distribution," Eur. Urol. **52**(6), 1653–1662 (2007).
12. T. Roose, "Challenges in imaging and predictive modeling of rhizosphere processes," Plant Soil **407**, 9–38 (2016).
13. C. C. Berry, "Progress in functionalization of magnetic nanoparticles for applications in biomedicine," J. Phys. D Appl. Phys. **198**, 22 (2009).

#273870 http://dx.doi.org/10.1364/BOE.7.004581
Journal © 2016 Received 15 Aug 2016; revised 25 Sep 2016; accepted 29 Sep 2016; published 17 Oct 2016

Biomedical Optics EXPRESS

14. Q. Pankhurst, N. Thanh, S. Jones, and J. Dobson, "Progress in applications of magnetic nanoparticles in biomedicine," J. Phys. D Appl. Phys. **42**(22), 224001 (2009).
15. V. S. Kalambur, B. Han, B. E. Hammer, T. W. Shield, and J. C. Bischof, "In vitro characterization of movement, heating and visualization of magnetic nanoparticles for biomedical applications," Nanotechnology **16**(8), 1221–1233 (2005).
16. T. Dreifuss, O. Betzer, M. Shilo, A. Popovtzer, M. Motiei, and R. Popovtzer, "A challenge for theranostics: is the optimal particle for therapy also optimal for diagnostics?" Nanoscale **7**(37), 15175–15184 (2015).
17. T. Reuveni, M. Motiei, Z. Romman, A. Popovtzer, and R. Popovtzer, "Targeted gold nanoparticles enable molecular CT imaging of cancer: an in vivo study," Int. J. Nanomedicine **6**, 2859–2864 (2011).
18. V. Adi, R. Arkady, B. Yevgeny, D. Hamootal, P. Rachel, and Z. Zeev, "manipulated magnetic nano particles for photonic biomedical mapping," Nanosci. Nanotechnol. Lett. **7**, 1–9 (2015).
19. H. Deramond, N. T. Wright, and S. M. Belkoff, "Temperature elevation caused by bone cement polymerization during vertebroplasty," Bone **25**(2 Suppl), 17S–21S (1999).
20. 20. Ag, L. C. "Technical Reference Guide Protocol for Performing a Trypan Blue Viability Test," BioResearch 2–3.
21. NEXCELOM-Innovation and Expertise in the Science of Cell Counting. at <http://www.nexcelom.com/Applications/measure-cell-viability-using-trypan-blue-or-AOPI.php>
22. Z. Zalevsky, Y. Beiderman, I. Margalit, S. Gingold, M. Teicher, V. Mico, and J. Garcia, "Simultaneous remote extraction of multiple speech sources and heart beats from secondary speckles pattern," Opt. Express **17**(24), 21566–21580 (2009).
23. U. Werner, K. Giese, B. Sennhenn, K. Plamann, and K. Kölmel, "Measurement of the thermal diffusivity of human epidermis by studying thermal wave propagation," Phys. Med. Biol. **37**(1), 21–35 (1992).
24. A. Welch, "The thermal response of laser irradiated tissue," IEEE J. Quantum Electron. **20**(12), 1471–1481 (1984).
25. J. T. Lin, "Selective cancer therapy using IR-laser-excited gold nanorods," SPIE Newsroom **2–4**, 2507 (2010).
26. D. G. Jay, "Selective destruction of protein function by chromophore-assisted laser inactivation," Proc. Natl. Acad. Sci. U.S.A. **85**(15), 5454–5458 (1988).
27. S. Wang, Y. Zhou, J. Tan, J. Xu, J. Yang, and Y. Liu, "Computational modeling of magnetic nanoparticle targeting to stent surface under high gradient field," Comput. Mech. **53**(3), 403–412 (2014).
28. J.-T. Lin, Y.-L. Hong, and C.-L. Chang, "Selective cancer therapy via IR-laser-excited gold nanorods," Medicine (Baltimore) **7562**, 75620R (2010).
29. Z. G. Forbes, B. B. Yellen, D. S. Halverson, G. Fridman, K. A. Barbee, and G. Friedman, "Validation of High Gradient Magnetic Field Based Drug Delivery to Magnetizable Implants Under Flow," IEEE Trans. Biomed. Eng. **55**(2), 643–649 (2008).
30. C. L. Ondeck, "Theory of magnetic fluid heating with an alternating magnetic field with temperature dependent materials properties for self-regulated heating," J. Appl. Phys. **105,** 07B324 (2009).
31. K. Yang, L. Hu, X. Ma, S. Ye, L. Cheng, X. Shi, C. Li, Y. Li, and Z. Liu, "Multimodal imaging guided photothermal therapy using functionalized graphene nanosheets anchored with magnetic nanoparticles," Adv. Mater. **24**(14), 1868–1872 (2012).
32. D. Zhu, F. Liu, L. Ma, D. Liu, and Z. Wang, "Nanoparticle-based systems for t(1)-weighted magnetic resonance imaging contrast agents," Int. J. Mol. Sci. **14**(5), 10591–10607 (2013).
33. D. G. Cahill, W. K. Ford, K. E. Goodson, G. D. Mahan, A. Majumdar, H. J. Maris, R. Merlin, and S. R. Phillpot, "Nanoscale thermal transport," J. Appl. Phys. **93**(2), 793–818 (2003).
34. P. Van Den Berg, A. T. De Hoop, A. Segal, and N. Praagman, "A Computational Model of the Electromagnetic Heating of Biological Tissue with Application to Hyperthermic Cancer Therapy," IEEE Trans. Biomed. Eng. **30**, 797–805 (1983).
35. R. Ludwig, M. Stapf, S. Dutz, R. Müller, U. Teichgräber, and I. Hilger, "Structural properties of magnetic nanoparticles determine their heating behavior - an estimation of the in vivo heating potential," Nanoscale Res. Lett. **9**(1), 602 (2014).
36. K. Du, Y. Zhu, H. Xu, and X. Yang, "Multifunctional magnetic nanoparticles: Synthesis modification and biomedical applications," Prog. Chem. **23**, 2287–2298 (2011).
37. Y. El Mendili, F. Grasset, N. Randrianantoandro, N. Nerambourg, J.-M. Greneche, and J.-F. Bardeau, "Improvement of thermal stability of maghemite nanoparticles coated with oleic acid and oleylamine molecules: Investigations under laser irradiation," J. Phys. Chem. C **119**(19), 10662–10668 (2015).
38. K. Yang, H. Xu, L. Cheng, C. Sun, J. Wang, and Z. Liu, "In vitro and in vivo near-infrared photothermal therapy of cancer using polypyrrole organic nanoparticles," Adv. Mater. **24**(41), 5586–5592 (2012).
39. K. Maier-Hauff, R. Rothe, R. Scholz, U. Gneveckow, P. Wust, B. Thiesen, A. Feussner, A. von Deimling, N. Waldoefner, R. Felix, and A. Jordan, "Intracranial thermotherapy using magnetic nanoparticles combined with external beam radiotherapy: Results of a feasibility study on patients with glioblastoma multiforme," J. Neurooncol. **81**(1), 53–60 (2007).
40. C. Tsouris and T. C. Scott, "Flocculation of Paramagnetic Particles in a Magnetic Field," J. Colloid Interface Sci. **171**(2), 319–330 (1995).
41. W. R. Chen, R. L. Adams, K. E. Bartels, and R. E. Nordquist, "Chromophore-enhanced in vivo tumor cell destruction using an 808-nm diode laser," Cancer Lett. **94**(2), 125–131 (1995).
42. B. J. Tromberg, N. Shah, R. Lanning, A. Cerussi, J. Espinoza, T. Pham, L. Svaasand, and J. Butler, "Non-invasive in vivo characterization of breast tumors using photon migration spectroscopy," Neoplasia **2**(1-2), 26–40 (2000).

Biomedical Optics EXPRESS

43. J.-T. Lin, Y.-S. Chiang, G.-H. Lin, H. Lee, and H.-W. Liu, "In Vitro Photothermal Destruction of Cancer Cells Using Gold Nanorods and Pulsed-Train Near-Infrared Laser," J. Nanomater. **2012**, 1–6 (2012).
44. D. O. Lapotko and V. P. Zharov, "Spectral evaluation of laser-induced cell damage with photothermal microscopy," Lasers Surg. Med. **36**(1), 22–30 (2005).
45. Y. Zhang, Y. Guo, P. Quirke, and D. Zhou, "Ultrasensitive single-nucleotide polymorphism detection using target-recycled ligation, strand displacement and enzymatic amplification," Nanoscale **5**(11), 5027–5035 (2013).
46. M. A. Nash, J. J. Lai, A. S. Hoffman, P. Yager, and P. S. Stayton, "'Smart' Diblock Copolymers as templates for magnetic-Core Gold-Shell Nanoparticles Synthesis," Nano Lett. **10**, 85–91 (2011).
47. J. M. El Khoury, D. Caruntu, C. J. O' Connor, K.-U. Jeong, S. Z. D. Cheng, and J. Hu, "Poly(allylamine) stabilized iron oxide magnetic nanoparticles," J. Nanopart. Res. **9**(5), 959–964 (2007).

1. Introduction

Photo-thermal therapy (PTT) is a minimally-invasive therapeutic strategy that destroys cancer cells using photon energy converted into heat [1–4]. One of the main PTT procedures involves dispersion of magnetic particles (MNPs) throughout the target tissue, and subsequent application of an external alternating magnetic field (AMF) of sufficient strength and frequency to induce heating of the particles. Heat is generated by different mechanisms, including hysteresis loss, N´eel relaxation time (the time between two temperature-induced random magnetization flips of super-paramagnetic nanoparticles) and Brown relaxation (rotation through frictional interaction between the particle and its surrounding medium) [3–5]. This heat conducts into the immediate surrounding of the diseased tissue, and maintenance of the temperature above the therapeutic threshold of 42°C for at least 30 min generally leads to destruction of the cancer site [3,4].

Although PTT was shown to be effective, various technical and physical limitations of currently available hyperthermia systems, including magnetic and laser-based systems, prevent adequate heating of some tissues. For instance, common electromagnetic devices for magnetic hyperthermia are generators in the frequency range of 50kHz–1MHz, with magnetic field amplitudes up to a few tens of kAm^{-1} [6–8]. These parameters depend more on the technical availability of the generators used, rather than on theoretical predictions for optimized specific absorption rate [8]. Lasers, which are typically used as the energy sources for PTT, are limited to treatment of superficial tumors; this is because human tissue shows strong extinction coefficients in the visible range of the optical spectrum [9], thus the maximum optical penetration depth achievable in human tissues is within the range of a few centimeters [10]. Moreover, laser light energy is absorbed by both healthy and cancerous tissues, leading to reduced efficacy of heat delivery within the tumor, and increased non-specific damage to adjacent tissues.

Laser intensity and energy fluency are additional parameters that need to be considered for optimal PTT. The laser intensity (laser power divided by laser spot area) can be controlled by adjusting the laser power and/or focal area. On the other hand, laser fluency provides a measure of the total energy delivered to the bio-system per unit area, and can be adjusted through the irradiation time and/or laser intensity. The threshold laser intensity required to achieve cell destruction depends on a large variety of parameters, including cell type, the type of nanoparticles used as PTT agents, number of nanoparticles uptaken by the cells, and environmental conditions [3,12].

In the present study, we suggest a novel method that can utilize lower laser intensity [12], reduce the exposure time to laser light, and provide more rapid and efficient cell destruction. To this end, we employed a dual method of heating, which combines laser irradiation together with AMF at low frequency and amplitude to produce MNP oscillations. The oscillations contribute to the rate of temperature rise of the cells. This method is based on the theory that external AMF induces the flowing of currents within MNPs; the amount of current is proportional to the size of the magnetic field and the size of the object. Concomitantly with current flow, the metal resists the flow and thereby its temperature rises, a process termed inductive heating. Therefore, when a magnetic fluid is exposed to AMF, the particles become powerful heat sources [11,12]. To approximate the overall theoretical temperature rise by radiative heat transfer, we developed a one-dimensional model and compared it to our experimental results herein. The theoretical model computes the heat diffusion equation with

Biomedical Optics EXPRESS

fixed laser fluency and an initial condition of T initial = 37°C. To this model we added a model that takes into account the heat generated from the particle movement, without the eddy currents generated and the hysteresis losses in the magnetic bulk. Due to the superparamagnetism properties of the magnetite core (Fe_3O_4) MNPs [9,10] used herein, these phenomena are peripheral, and the main mechanism that contributes to the heating of the particles is relaxation losses.

Herein we examined an *in vitro* proof of concept of our new and simple cancer cell destruction technique. Using a head-and-neck cancer cell line sample, we assessed the effect of treatment with laser irradiation and an external AMF field on the near-surface temperature profile, and compared it to that of the theoretical model. In addition, we examined the effect of different MNP concentrations, of different laser fluencies and of AMF treatment combined with laser, on cancer cell death.

2. Materials and methods

2.1 Study design

The setup included a green laser (532 nm) that illuminated a sample of A431 cells in the presence of MNPs, a mirror that focused the laser beam directly on the sample vial, and an electromagnet, which produced the magnetic field in order to achieve MNP movement. All heating experiments were repeated 3-5 times. A real-time temperature monitoring device was used to measure surface temperature, which was measured and compared with the theoretical calculation (though we note that theoretical prediction is possible only in an ideal situation). Cell viability after treatment was measured using a Trypan blue assay and an MTT assay.

2.2 In vitro experiments

Cell culture: A431 head and neck cancer cells (2.5×10^6) were derived from the American type culture collection [16], and were maintained in 5 mL Dulbecco's modified Eagle's medium containing 5% fetal calf serum, 0.5% penicillin, and 0.5% glutamine. For experiments, cells were added to vials at a density of X cells/ml in 1 ml medium solution. The first group was incubated with 50 μL of MNPs (5 mg/mL) for 30 minutes at 37°C. After incubation, the medium was washed twice with phosphate buffered saline followed by addition of 1 mL of aqua regia [17]. After evaporation of the acid, the sediment was dissolved in 5 mL 0.05 M hydrochloride.

AMF treatment: We used the particle and electrical system parameters that yielded the best correspondence of MNPs with the magnetic field, as shown in our previous work [18]. Briefly, AMF was carried out by applying 4 volt to a constructed coil at fixed frequency of 3 Hz, with a magnetic field of 6.2G (measured by Bell 5170 gaussmeter, Berg engineering). See System Specifications (below) for further details.

MNPs: MNPs (Chemicell, Berlin, Germany) with a radius of 50 nm and an amine shell (Fig. 1) were used, at a concentration range of 2-10 mg/ml, as detailed in each experiment.

Biomedical Optics EXPRESS

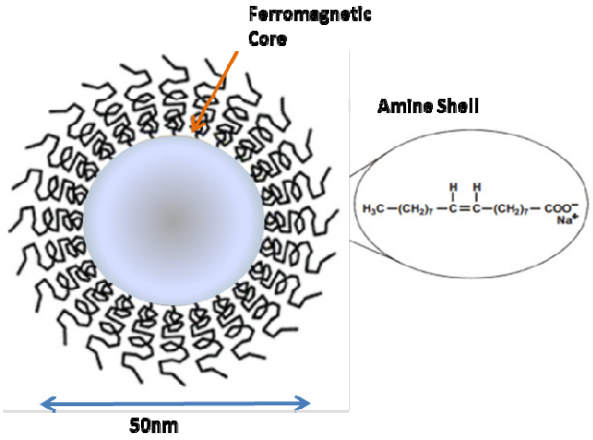

Fig. 1. Scheme of 50 nm Chemicell, ferromagnetic core coated with an amine shell.

Laser treatment: Each sample was illuminated with green DPSS laser at wavelength of 532nm (Photop DPGL-2100), with an output optical power of 30-80 mW. See System Specifications (below) for further details.

Temperature Measurements: Real-time temperature of the cells and MNP suspension (1 mL) under various AC magnetic fields was measured by T-type thermocouples (Omega Engineering Inc., Stamford, CT, USA) inserted into the sample vial and secured with polyimide tape, as seen in Fig. 3(a). T-type thermocouples were chosen because they are inexpensive, small, and work well in an oxidizing environment [19]. The temperature was recorded every 5 sec, and used to generate heating profiles for each sample.

Trypan blue assay: X µl of cell suspension was taken and mixed with an equal volume of 0.4% Trypan blue (COMPANY). The solution was mixed thoroughly and allowed to stand for 5 min at room temperature. Cell viability was determined by counting the unstained (live) cells under a microscope (Leica) [16,17]. The total number of live cells in a sample at each time point was calculated by counting cells under the microscope in four 1 x 1 mm squares of one chamber and determining the average number of cells per square.

MTT assay: For the MTT assay (TOX-1, Sigma-Aldrich, USA), we measured $74e^4$ cells/vial, either with A431 cells only or cells incubated with MNPs for 48 hrs. Cells were plated at 100,000/well in a 24-well plate and allowed to adhere overnight. MNPs were suspended in media at 1 mg Bi/mL, sonicated, and 10-fold dilutions in media were made down to 0.1 µg/mL. MNP solution (5 mg/ml) was added to each vial. Controls received fresh media only. After 2 days of co-incubation, MNP solution was replaced with mixture of 400 µL media and 40 µL of MTT powder (1-(4,5-Dimethylthiazol-2-yl)-3,5-diphenylformazan, Sigma) at 5 mg/mL in PBS. Two hours later, media was aspirated and 1 mL of DMSO (Fisher) was added to each vial. 50 µL was immediately transferred to a 96-well plate and absorbance was measured by a spectrophotometer at 570 nm (SpectraMax 190, Molecular Devices), using DMSO-only wells to establish baseline. For each experiment, 5 wells were tested per bismuth concentration, and experiments were repeated twice. Optical density measurements were normalized to wells containing cells unexposed to MNPs.

2.3 System specifications

The heating equipment was composed of an electro-magnet (for AMF treatment) made of copper coil surrounding an E Ferrite core, with 30 Ω resistance (L1). The coil is connected to a waveform generator (AFG 3022B, Tekronix, Inc., USA), connected to an oscilloscope (TDS 1002 Tekronix, Inc, USA) that shows the amplitude and frequency on a screen (CH1, see Fig. 2). Another resistor (10 Ω, R1) is connected to the coil, the generator and the scope (CH2 in Fig. 2).

Biomedical Optics EXPRESS

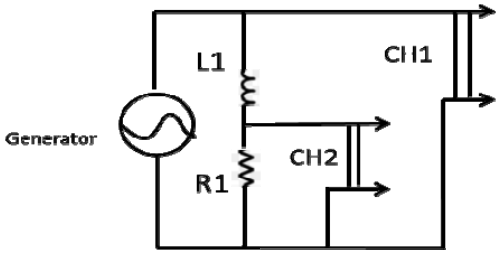

Fig. 2. Scheme of the electrical circuit. An electro-magnet (for AMF treatment) made of copper coil surrounding an EC Ferrite core (30 Ω resistance, L1) is connected to a waveform generator, connected to an oscilloscope that shows the amplitude and frequency on a screen (CH1). Another resistor (10 Ω, R1) is connected to the coil, the generator and the scope (CH2).

The magnetic field was controlled by adjusting the voltages and frequencies in the waveform generator. A schematic illustration of the experimental setup is shown in Fig. 3(a) and a schematic illustration of the magnetic field is shown in Fig. 3(b).

The laser was set in a straight angle of ~90° towards a mirror set with an oblique angle of ~45° above the sample, thus the laser beam illuminates straight onto the sample. This was done to avoid collecting directly transmitted illumination [22].

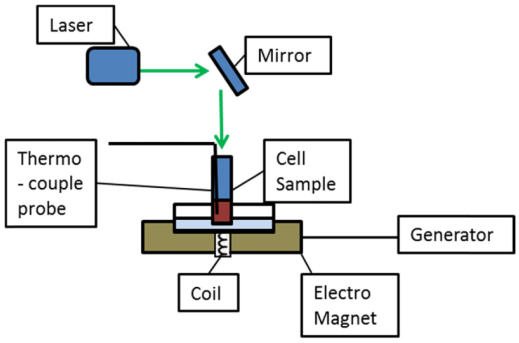

(a)

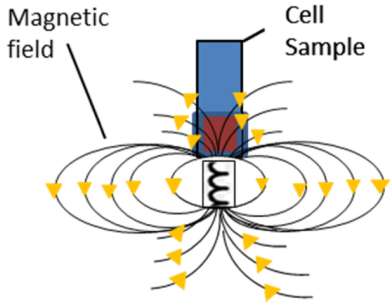

(b)

Fig. 3. (a) Schematic illustration of the experimental setup. The cell sample with an inserted and secured thermocouple probe was placed on top of the AMF system (including an electromagnet, coil and generator). The laser was set above the sample, in a straight angle of ~90° towards a mirror set with an oblique angle of ~45° above the sample, thus the laser beam illuminated straight onto the sample. (b) Schematic illustration of the magnetic field. The magnetic field was controlled by adjusting the voltages and frequencies in the waveform generator.

Biomedical Optics EXPRESS

2.3 Modeling

Approximate solution of radiative heat transfer theory, which is a one-dimensional model, was used to assume the cells and the MNP solution temperature change (∂T) due to laser heating. This is described by a heat diffusion equation:

$$\frac{\partial^2 T(x,t)}{\partial x^2} = \frac{1}{\alpha}\frac{\partial T(x,t)}{\partial T} - H(x,t) \tag{1}$$

where x is the laser propagation direction along the depth of the cell and MNPs solution, H is the source density, ∂T is the partial temperature differential and ∂t is the partial time differential, α is the thermal diffusivity of the solution, which can be expressed by:

$$\alpha = \frac{k}{\rho C_P} \tag{2}$$

where k is the thermal conductivity, ρ is the density and C_p is the specific heat capacity. The deposition of heat is assumed to be given by the absorption of energy from a plane radiation field of intensity, I, propagating along the x-axis. Then the source density H of deposited heat can be expressed as:

$$H = \frac{\partial I(x,t)}{\partial x}. \tag{3}$$

The thermal properties of materials, in general, are determined from the time dependence of the temperature elevation which is observed after the deposition of the heat [19,20]. With fixed laser fluency the source density can be described by:

$$H = \frac{AF}{D} e^{-Ax} \tag{4}$$

where D is the thermal diffusivity of the solution, F is the laser fluency, A is the extinction coefficient, which is a function of the absorption and scattering coefficient [21,22]. The heat diffusion will be calculated numerically with the initial condition of $T_{initial}$ = 37°C and the boundary condition of:

$$\frac{\partial T}{\partial t}(x=0) = \frac{DT(x,0)}{h} \tag{5}$$

where h is the heat transport coefficient (resulted by the air convection through the sample). We measured the near-surface temperature, at x = 2.3mm, and the temperature differential was 5°C, with a bandwidth of 0.1°C, using diode lasers at 532 nm for various output optical power of 30-80mW and fit parameters of D = 0.0045 (WC/cm), α = 0.00149 (cm^2/s), and h = 0.05 (WC/cm^2) [23,24]. This theoretical model estimates the temperature increase rate of the solution of cells and MNPs under laser illumination, without considering the stimulus of the rate influenced by the external magnetic field, which results in particle oscillations in the solution.

In order to take into account the temperature rise caused by the MNP movement, a theoretical model was developed based on Kalambur et al. [7], which considers the forces on the MNPs as a one-dimensional problem along the centerline of the magnet at steady state, neglecting diffusion and the corresponding random force [29]. Due to the MNPs' size (50 nm), the eddy currents generated and the hysteresis losses in the magnetic bulk are peripheral and the significant mechanism that contributes to the heating of these particles is relaxation losses in superparamagnetic single-domain magnetic materials [5, 25–27]. The power generated, being a strong function of the size and is given by:

Biomedical Optics EXPRESS

$$P = \pi\mu_0\chi_0 H_0^2 f \frac{2\pi f\tau}{1+(2\pi f\tau)^2} \quad (6)$$

where μ_0 is the permeability of free space, χ_0 is the magnetic susceptibility, H_0 and f are the amplitude and frequency of the applied alternating magnetic field, respectively, and τ is the effective time constant that mediates the relaxation modes that lead to heat generation, characterized by the time constants (N´eel time constant and Brownian time constant [15]). As seen in the literature, presenting heat generation model has to consider certain complications; the effective temperature rise observed is the suspending medium macroscopic temperature change [7].There is a strong dependence between the heat response and various medium solutions and much needs to be understood before a quantitative model can be developed to correlate the two [5,33,34].

The heat from the relaxation losses leads to a rate of temperature rise given by:

$$\frac{\Delta T}{\Delta t} = \frac{P}{\rho C_P} \quad (7)$$

where ρ is the weighted density (~1.25 g/cm^3) and C_p is the weighted specific heat capacity of the system considering the MNP temperature (103.4 + 0.69T - 1.77e6/T^2) [29,30] within the carrier medium [27]. The overall theoretical temperature rise combines Eq. (5) and 7, as given by:

$$\frac{dT}{dt}(x=0) = \frac{DT(x,0)}{h} + \frac{P}{\rho C_P}. \quad (8)$$

The first term of the equation relates to the laser heating. By substituting the relevant parameters (D and h, as mentioned above) this part is less dominant by two orders of magnitude than the second term, i.e., MNP oscillation [30,31].

The feasibility of this approach is validated by comparing the capture efficiency of laser and MNPs without movement to that with movement. A parametric study was performed on the capture efficiency of MNP movement.

2.4 Statistical analysis

A t-test was conducted to assess statistical differences between two groups.

3. Results

3.1 Effect of AMF and laser irradiation on temperature change of cells over time

To examine the effect of AMF and laser irradiation on A431 cells in solution (1 ml medium), we measured the temperature profiles of the near-surface cells under several conditions. The temperature was measured every 5 sec, using T-type thermocouples (as detailed in Methods).

We first assessed the effect of AMF on temperature reading by the thermocouple probe. The temperature of A431 cell solution, without MNPs, was measured for 10 mins, followed by application of the AMF on the solution for 10 min (with all other conditions identical). No statistically significant difference was found in the temperature of the solution with or without AMF treatment (37.31°C ± 0.07, 37.27°C ± 0.09), (n = 50); independent-samples t-test, t(50) = 0.43, p = 0.66). These results indicate that applying AMF on the cell solution has no effect on temperature reading by the probe.

We next examined the effect of AMF on the rate of temperature increase from the initial temperature of 37°C to the therapeutic threshold of 42°C (5°C temperature change), in a cell solution with MNPs. A431 cells (in 1 ml medium) with 50 nm MNPs (5 mg/ml) were illuminated by laser beam irradiation (30 mW), with or without AMF (3 Hz, 300 mW) (n = 5 samples per group). We also measured the temperature of cell solution without laser irradiation, to understand the laser heating contribution. Figure 4 shows the gradual increase in sample temperature over 5 min of treatment. The samples treated with laser and AMF

Biomedical Optics EXPRESS

reached the 42°C goal after 4.5 min of treatment, while the samples treated with laser irradiation alone increased to a temperature of 38.1°C at the 4.5 min time point. Thus, AMF improves the temperature increase rate by 10.2% (for the combination of AMF and laser). The sample treated with AMF and without laser, reached 39°C. Thus, The laser illumination improves the temperature increase rate by 7.7%. To examine the effect of AMF treatment on the MNPs, without cell solution we measured the temperature profile of deionized water with added MNPs (5 mg/ml) and without cells, treated with AMF (3 Hz, 300 mW) and laser (30 mW) (n = 5 samples per group). The deionized water exhibited a temperature increase that parallels that of the cell solution treated with AMF.

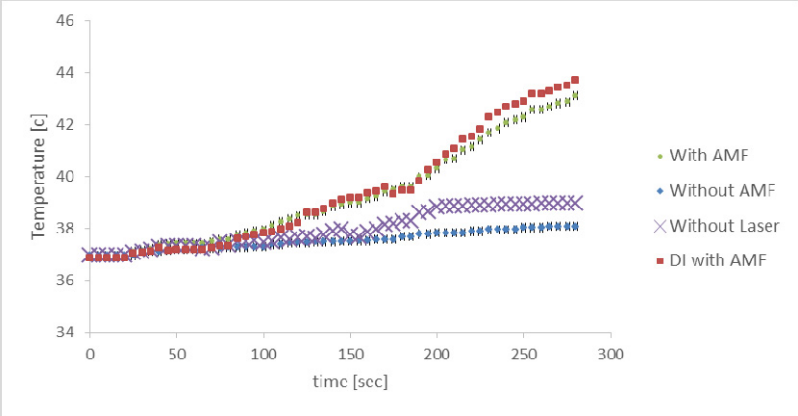

Fig. 4. Temperature of the cell sample (blue, green) and deionized water (DI) sample (red) with 5 mg/ml particles, treated with 30 mW laser irradation, with or without alternating magnetic field (AMF) and cell sample (purple) treated with AMF and without laser, over time. The sample reached a the goal temperature of 42°C when treated with laser combined with AMF after 4.5 min of treatment, while the sample treated with laser alone reached only 38.1°C. DI showed a temperature profile similar to that of the cell solution treated with AMF.

To examine the effect of laser irradiation on temperature change, cells in the presence of 50 nm MNPs (5 mg/ml) were treated with AMF and with laser illumination at fluencies of 30, 50 or 80 mW. These experiments were carried out at very low laser power to minimize possible sample deterioration or phase transformation with operating time, as seen in the literature [37]. The change in near surface temperature (∂T) was measured over 5 min. As demonstrated in Fig. 5, there was no significant difference in temperature change of cells treated with the highest laser fluency as compared to the lower fluencies, as might have been expected from the theoretical heat diffusion equation Eq. (4). The different laser fluencies had a minor contribution to the overall source density. Laser fluency is a position-dependent value. It is often highest on the beam axis, and lower at positions somewhat further from that axis. It is meaningful only in combination with relatively longer irradiation time than that we used here [12]. We assume that the fluency dependence would be more significant with a wider and stronger range of fluencies.

Biomedical Optics EXPRESS

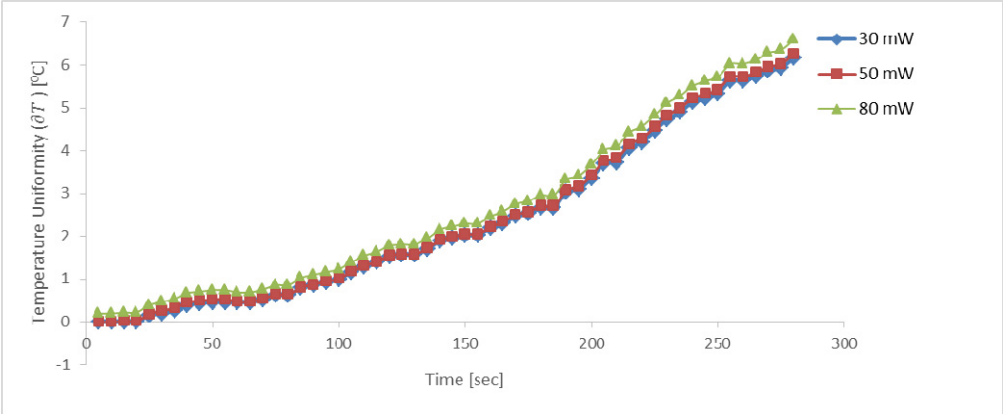

Fig. 5. Profiles of temperature change (∂T) at the sample surface, with 5 mg/ml particles, during treatment with 30-80 mW laser irradiations and AMF (3 Hz, 300 mW). No significant difference in temperature change was found between the different laser fluencies.

We next compared the temperature change (∂T) profile of a cell solution with MNPs (5 mg/ml), treated with 30 mW laser irradiation and AMF, to the overall theoretical temperature rise as given in Eq. (8) (Fig. 6). Our findings demonstrate a more rapid rate in temperature rise, of about ~50%, in the cell sample as compared to the theoretical model (Fig. 6).

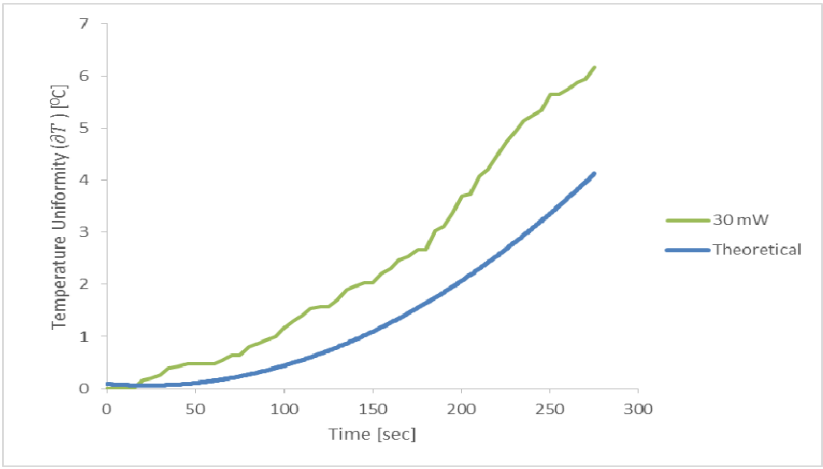

Fig. 6. .Profile of temperature change (∂T) at the sample surface, with 5 mg/ml particles, 30 mW laser irradiation and 3 Hz, 300 mW AMF ('30 mW'; green line). The theoretical curve (blue) was obtained from the heat diffusion equation solution Eqs. (1)-(5).

3.2 Effect of AMF and laser irradiation on cell viability

Next, we examined the effect of AMF and laser irradiation (30 mW) on the number of live cells in a cell sample with 5 mg/ml particles, while concurrently measuring near-surface temperature, throughout the 5-min treatment period. The number of live cells was measured every 60 seconds using trypan blue. Figure 7 shows a gradual decrease in the number of live cells over time, until they reached ~50% of the initial amount by the end of the 5-min treatment, concurrently with a gradual, 5-degree rise in the near-surface temperature.

Biomedical Optics EXPRESS

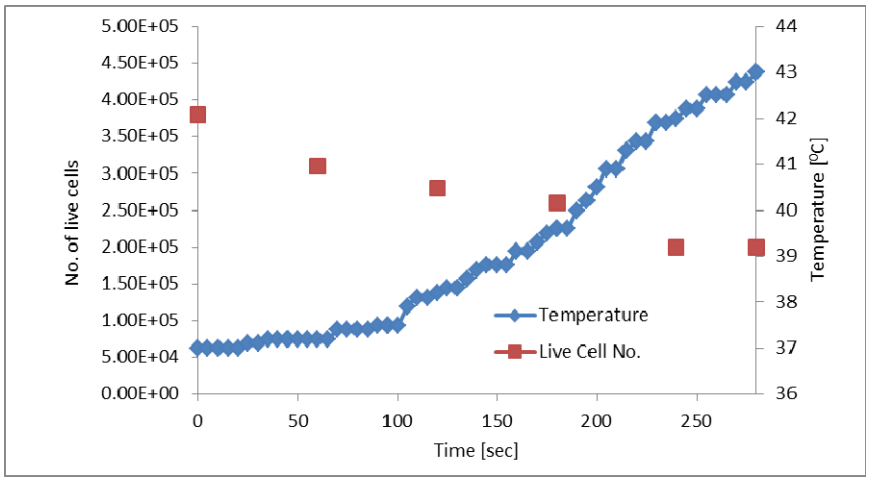

Fig. 7. Temperature and number of live cells over time in a sample with 10 mg/ml particles, treated with 30 mW laser irradiation and 3 Hz, 300 mW AMF. As the temperature of the sample rose, the number of live cells decreased over the 5-min treatment, up to ~50% of the initial amount.

We continued by examining the effect of MNP presence and AMF treatment on cell viability. To this end, we assessed A431 cell solutions under several conditions: cell solutions treated with AMF and 30 mW laser irradiation, either with or without 10 mg/ml MNPs; a cell solution with 10 mg/ml MNPs, treated with 30 mW laser irradiation but no AMF; and lastly, a cell solution with 10 mg/ml MNPs treated with AMF but without laser irradiation (5 min treatment in all conditions). Figure 8 shows the total number of cells and the number of dead cells in each solution. We found that dead cells appeared only in the two solutions that contained MNPs and were treated with AMF, irrespective of laser treatment. The particles and laser + AMF treatment combination achieved 41% cell death after 5 min, while the solution with particles treated with AMF alone reached 26% cell death. This indicates that the cause of cell death was not due solely to the temperature increase (to 42°C), but rather to the combination of AMF-induced particle motion and temperature increase.

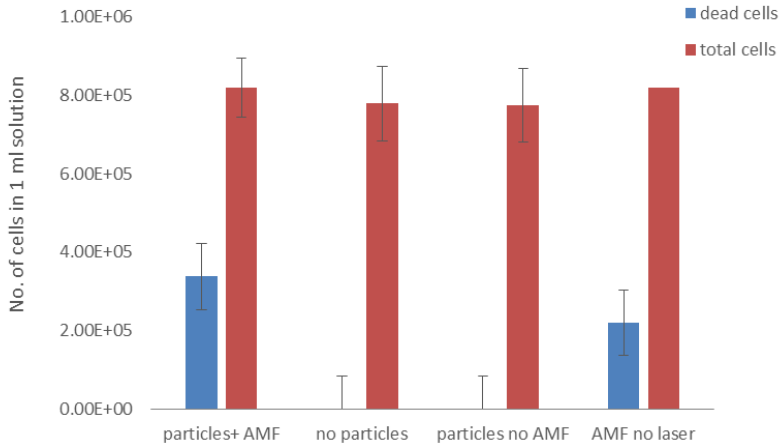

Fig. 8. Number of cells in A431 cell solution (1 ml). Columns left-to-right: Cells with 10 mg/ml particles and treatment with 30 mW laser irradiation + 3 Hz, 300 mW AMF; cells treated with laser + AMF, without particles; cells with particles, treated with laser only; and cells with particles and treated with AMF only. Treatment duration was 5 min. Dead cells were found only in cells solutions that contained particles and were treated with AMF, irrespective of laser treatment.

Biomedical Optics EXPRESS

We next examined the effect of particle concentration on cell death induced by our combined treatment. Cell solutions with 2-10 mg/ml MNP were treated with 30 mW laser irradiation and AMF for 5 min. As shown in Fig. 9, we found that the 10 mg/ml solution reached 41% cell death, while 2 mg/ml induced only 28% cell death. The solutions with 7 and 5 mg/ml reached 38.8% and 34.2% cell death, respectively.

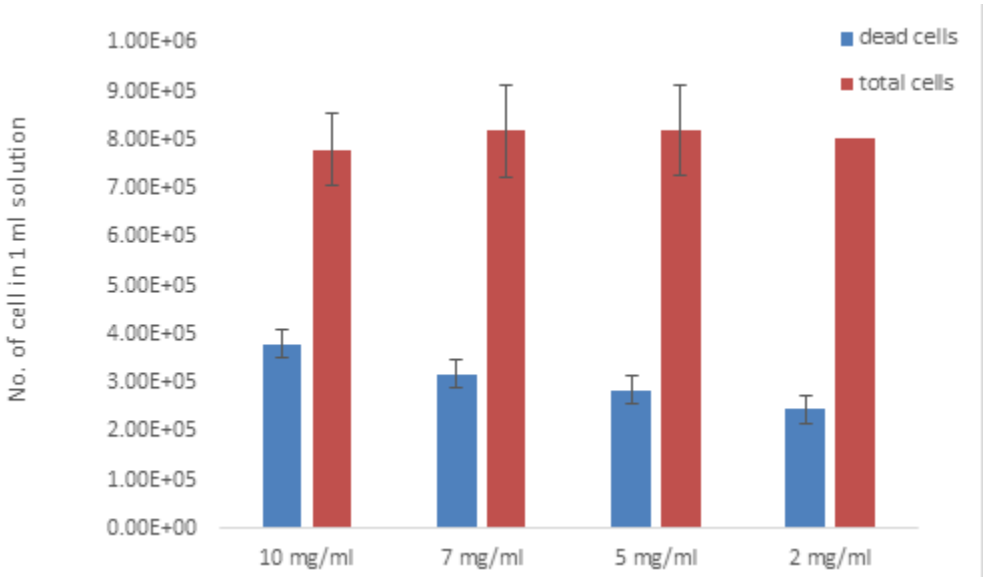

Fig. 9. Number of cells with different particle concentrations (2-10 mg/ml) in 1 ml solution after 30 mw laser irradiation and AMF (3 Hz, 300 mW) for 5 min. The amount of dead cells increased as the concentration of MNPs increased.

To determine whether MNP presence alone can cause cell death, we examined under microscope the viability of A431 cells with 10 mg/ml MNPs, with or without laser irradiation and AMF treatment (n = 3 plates per group, 10^6 cells/plate). Cells incubated for 48 hrs with MNPs showed viability similar to that of untreated negative control cells (Fig. 10(a)-10(b)). However, cells with MNPs that were treated with laser irradiation and AMF (5 min; cells examined immediately after treatment) showed complete cell death (Fig. 10(c)).

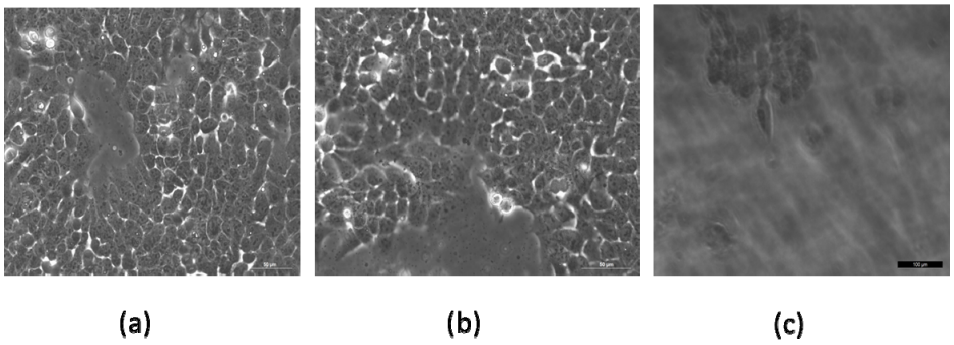

Fig. 10. Cell viability test. 74e4 A431 cells in Petri dishes containing (a) untreated cells, (b) cells incubated with 10 mg/ml MNPs for 48 hrs, (c) cells with 10 mg/ml MNPs examined immediately after 5 min of 30mW laser illumination and AMF (3 Hz, 300 mW) treatment. Only cells with MNPs and treated with laser + AMF showed complete cell death. Imaged by Leica microscope X20.

We further examined the effect of MNPs on A431 cell viability using an MTT assay, examining the absorbance of untreated cells and cells incubated with MNPs (n = 5/group). An

Biomedical Optics EXPRESS

independent-samples t-test showed no significant difference in the absorbance scores of untreated cells (M = 0.094, VAR = 9.84e5) and cells with MNPs (M = 0.063, VAR = 3.48e5); t(4) = 2.1, p = 0.13. Taken together, these results indicate that MNPs alone do not affect cell viability.

The results of all experiments are summarized in Tables 1 and 2.

Table 1. The effect of AMF and different laser fluencies on temperature change of near-surface A431 cells.

AMF [on/off]	Laser fluencies [mW]	MNP Concentration [mg/ml]	Temperature after 5 min [^{0}c]
On	30	5	42
Off			38.1
On	30	5	42.6
	50		42.7
	80		42.9

Table 2. The effect of the treatments and different MNP concentrations on A431 cell death.

AMF [on/off]	Laser fluencies [mW]	MNP Concentration [mg/ml]	Dead cells [%]
On	30	10	41
	30	-	No
	-	10	26
Off	30	10	No
On	30	10	41
		7	38.8
		5	34.2
		2	28

4. Discussion

Herein, we show that an A431 cell solution reached the therapeutic threshold temperature of 42°C after 4.5 min with AMF treatment, while treatment with laser only and without AMF did not sufficiently raise the temperature. The temperature of 42°C did not cause cell death on its own, as seen in cells treated with laser only, or with AMF + laser but no MNPs, yet this goal was reached after only 5 min of combination treatment in the presence of particles, resulting in approximately half of the total cells dead, and after AMF alone, yielding approximately one quarter dead. The short treatment time indicates that the cause of cell death was due to particle motion in combination with, and not solely due to, the temperature rise.

The combination of MNPs with AMF and laser produced an effect over 5 min of treatment, which is more rapid than currently existing treatments that generally require 30 min of heating or more [32,33]. This finding suggests that our method can reduce exposure time to laser light energy, which is commonly used in PTT and absorbed by both healthy and cancerous tissues. In addition, the actual temperature increase of the samples was 50% higher than our theoretical model, which approximates the overall temperature rise by incorporating heat generation from particle oscillation and radiative heat transfer, although, as mentioned before, the model is a rough estimation [27,34,40]. However, we note that that the theoretical model does not take into account the combined effect of illumination-induced and oscillation-induced heating, which may explain the difference between practice and theory. Nonetheless, by consolidating the two factors in the present work, we achieved an improved heating effect, created by the laser flux combined with particle oscillation. This synergistic effect allows usage of lower laser intensity and lower AMF amplitude and frequency than those generally used for PTT in the literature [7,22,31–35].

Finally, we show that higher particle concentration causes higher cell death rate. We hypothesize that the temporal movement of the MNPs caused a higher cell destruction rate, with efficient results due to the short distance between the sample and the magnetic field source, and the combination of laser heating.

Biomedical Optics EXPRESS

Magnetite core MNPs used herein are biocompatible, and as super-paramagnetic nanoparticles, their magnetism depends upon the existence of an external magnetic field, which prevents their aggregation [9,10]. In addition, the functional groups of MNPs can easily create covalent coupling with antibodies or proteins that can target and selectively bind to the cancer cells [36–38]. MNPs also enhance proton relaxation of specific tissues, and thereby can be used contrast agents for magnetic resonance imaging (MRI) [32]. Thus, MNPs can serve as a multi-functional platform for cancer therapy, providing simultaneous tumor heating and imaging [1, 34]. These unique MNP features further emphasize the potential of our method for enhancing PTT, as targeted MNPs that reach specific tissue can induce cell death independently from that of the non-targeted tissue, via AMF combined with laser. Based on our previous study that showed that MNPs serve as contrast agents for a spackle-based detection method [18], herein we used the MNPs as distraction-mediator agents.

In summary, laser heating combined with MNP oscillation leads to more rapid and efficient cell death, demonstrating that the manipulated MNP technique can be a superior agent for PTT. As this method can be used to specifically target cells or other live tissue, it can provide a concentrated assembly for improved cell death capabilities.

Acknowledgment

The authors would like to thank Dr. Arkady Rudinzky for the technical support. The authors have no conflicts of interest to disclose.